

**Phospholipid-functionalized gold electrode for cellular membrane interface studies -  
interactions between DMPC bilayer and human cystatin C**

3 Paweł Niedziałkowski<sup>a\*</sup>, Przemysław Jurczak<sup>b,c,\*\*</sup>, Marta Orlikowska<sup>b</sup>, Anna Wcisło<sup>a</sup>, Jacek Ryl<sup>d</sup>, Tadeusz  
4 Ossowski<sup>a</sup>, Paulina Czaplewska<sup>c</sup>

5 <sup>a</sup> Department of Analytical Chemistry Faculty of Chemistry, University of Gdansk, Wita Stwosza 63,  
6 Gdańsk, 80-308, Poland

7 <sup>b</sup> Department of Biomedical Chemistry, Faculty of Chemistry, University of Gdansk, Wita Stwosza 63,  
8 Gdańsk, 80-308, Poland

9 <sup>c</sup> Specialist Laboratories, Intercollegiate Faculty of Biotechnology UG&MUG, Abrahama 58, Gdańsk, 80-  
10 307, Poland

11 <sup>d</sup> Division of Electrochemistry and Surface Physical Chemistry, Institute of Nanotechnology and Materials  
12 Engineering and Advanced Materials Center, Gdańsk University of Technology, Narutowicza 11/12,  
13 Gdańsk, 80-233, Poland

14 \* Correspondence to: P. Niedziałkowski, Department of Analytical Chemistry Faculty of Chemistry,  
15 University of Gdansk, Wita Stwosza 63, Gdańsk, 80-308, Poland

16 \*\* Correspondence to: P. Jurczak, Department of Biomedical Chemistry, Faculty of Chemistry, University  
17 of Gdansk, Wita Stwosza 63, Gdańsk, 80-308, Poland, Specialist Laboratories, Intercollegiate Faculty of  
18 Biotechnology UG&MUG, Abrahama 58, Gdańsk, 80-307, Poland

19 E-mail addresses [pawel.niedzialkowski@ug.edu.pl](mailto:pawel.niedzialkowski@ug.edu.pl), (P. Niedziałkowski), [przemyslaw.jurczak@ug.edu.pl](mailto:przemyslaw.jurczak@ug.edu.pl)  
20 (P. Jurczak)

21 **Abstract:** This work describes the electrochemical studies on the interactions between V57G mutant of  
22 human cystatin C (hCC V57G) and membrane bilayer immobilized on the surface of a gold electrode. The  
23 electrode was modified with 6-mercaptohexan-1-ol (MCH) and 1,2-dimyristoyl-sn-glycero-3-  
24 phosphocholine (DMPC). DMPC was used as a membrane mimetic for monitoring electrochemical changes  
25 resulting from the interactions between the functionalized electrode surface and human cystatin C. The  
26 interactions between the modified electrode and hCC V57G were investigated by cyclic voltammetry and  
27 electrochemical impedance spectroscopy in a phosphate buffered saline (PBS) containing  $\text{Fe}(\text{CN})_6^{3-/4-}$  as a  
28 redox probe. The electrochemical measurements confirm that fabricated electrode is sensitive to hCC V57G  
29 at the concentration of  $1 \times 10^{-14}$  M. The incubation studies carried out at higher concentrations resulted in  
30 insignificant changes observed in cyclic voltammetry and electrochemical impedance spectroscopy  
31 measurements. The calculated values of surface coverage  $\theta_R$  confirm that the electrode is equally covered  
32 at higher concentrations of hCC V57G. Measurements of wettability and surface free energy made it  
33 possible to determine the influence of individual structural elements of the modified gold electrode on its  
34 properties, and thus allowed to understand the nature of the interactions. Contact angle values confirmed  
35 the results obtained during electrochemical measurements, indicating the sensitivity of the electrode  
36 towards hCC V57G at the concentration of  $1 \times 10^{-14}$  M. In addition, the XPS spectra confirmed the  
37 successful anchoring of hCC V57G to the DMPC-functionalized surface.

38

39 **Keywords:** human cystatin C, DMPC, phospholipid, membrane, 6-Mercaptohexan-1-ol, electrode  
40 modification

## 41 **1. Introduction**

42 An amyloid is an insoluble, aggregated form of a protein or peptide, which assumes a fiber-like  
43 shape [1]. The process of accumulation and deposition of amyloid is a hallmark of amyloid diseases, a  
44 group of pathological states exhibiting various symptoms, e.g., Parkinson's or Alzheimer's disease. Up to  
45 date about forty amyloid-forming peptides and proteins were described [2]. Among them we find human  
46 cystatin C (hCC), a small size (120 amino acid-long) inhibitor of cysteine proteinases [3]. This protein with  
47 physiologic isoelectric point of pH 9.3 [4] can be found in all human body fluids at physiologically relevant  
48 concentrations [5]. Despite the physiological relevance of the wild-type hCC as a regulator of the activity  
49 of inter- and intramolecular cysteine proteases, its Leu<sup>68</sup>→Gln mutant is prone for accumulation, causing a  
50 dominant hereditary disorder called hereditary cystatin C amyloid angiopathy, a disease characterized by  
51 brain strokes and death of patients at a young age [6].

52 Even though the processes leading to amyloidogenic diseases are not crystal clear, it is known that  
53 protein oligomerization is a key feature of the amyloid formation. Research indicates that biological  
54 membranes have a great impact on the process of amyloidogenic proteins' oligomerization [7–9]. Up to  
55 date two possible mechanisms of protein oligomerization were proposed [10]. The first one assumes that  
56 the protein oligomerizes in extracellular matrix. The second, that the membrane is the interface which  
57 facilitates and accelerates the whole process. Both ideas involve different oligomeric states of a protein and  
58 finally lead to the formation of fibrils [10]. An annular oligomer is one of the oligomeric states on the route  
59 to the fibril formation. It may form channels in biological membranes disturbing their integrity, therefore it  
60 is indicated as a potential cause of toxicity of amyloidogenic proteins [10]. The formation of annular  
61 oligomers was observed for different amyloidogenic proteins *i.e.* amyloid  $\beta$  peptide [11], immunoglobulin  
62 light chain [12] and human cystatin C [13]. The interaction of toxic forms of hCC (the protein of our  
63 interest) with biological membranes is an interesting aspect of studies on amyloidogenic diseases and may  
64 be crucial in the context of describing the mechanisms causing them.

65 The studies on interactions between proteins and membranes are not a trivial task. Biological  
66 membranes are complex multi-component structures, therefore to facilitate experimental measurements  
67 natural membranes are often substituted with model structures including micelles, bicelles and liposomes  
68 [14,15]. Different methods involving the use of natural and model membranes have been developed. Among  
69 others we find surface plasmon resonance (SPR) [16], isothermal titration calorimetry (ITC) [17], nuclear  
70 magnetic resonance (NMR) spectroscopy[15], Fourier transform infrared spectroscopy (FTIR) [18],

71 hydrogen-deuterium exchange (HDX) mass spectrometry [19] or molecular dynamics (MD) simulations  
72 [20]. These techniques include also such interesting concepts as monitoring of resonance frequency and  
73 energy dissipation on lipid covered quartz crystal (microbalance) resulting from a contact/interaction with  
74 a protein [21] or the use of anisotropy of nuclear interactions (solid-state NMR) to determine protein  
75 structure within solid or semi-solid lipid membrane structures [22]. Some of the methods applied for  
76 protein-membrane interactions present such a broad range of application or particular design, that they can  
77 be applied for studies on soluble proteins as well as protein aggregates and fibrils (*i.e.*, amyloid fibrils),  
78 which often prove to be tricky study objects due to their low solubility. These techniques comprise *i.a.* total  
79 internal reflection ellipsometry (TIRE) [23], Förster resonance energy transfer (FRET) [24], fluorescence  
80 imaging [25], quartz crystal microbalance applications [26] or MD simulations [27]. The technique which  
81 seems to be exploited the most in the field of protein-membrane interactions, regardless of the oligomeric  
82 state of the studied molecule, is atomic force microscopy (AFM). It allowed, *e.g.*, to visualize aggregation  
83 of  $\alpha$ -synuclein on a surface of phospholipid bilayers and (combined with computational modeling) to  
84 present a possible model of aggregation of this amyloidogenic protein [28]. AFM imaging was also applied  
85 to visualize the formation of annular oligomers (amyloid fibril precursors) forming transmembrane  
86 channels [29].

87 All the mentioned techniques shine bright in some aspects of application and falter in others. One  
88 of the greatest disadvantages of many mentioned above (*e.g.*, NMR, ITC, SPR) is their high cost, resulting  
89 from relatively high amount of protein/membrane material required for the measurement and/or high cost  
90 of the measurement itself. Therefore, here the application of electrochemical impedance spectroscopy (EIS)  
91 and cyclic voltammetry (CV) as methods for studies on protein-membrane interactions based on V57G  
92 mutant of hCC and the DMPC membrane mimetic is presented.

93 The hCC protein was previously detected with electrochemical methods including cyclic  
94 voltammetry (CV) and differential pulse voltammetry (DPV) on screen printed electrode modified with  
95 papain (cysteine protease) [30] or carbon electrode functionalized with graphene oxide-chitosan (GO-Chit)  
96 and with anti-cystatin C antibody [31]. The hCC was also detected with CV and DPV methods on glassy  
97 carbon electrode covered with aminoferrocene (Fc), graphene oxide (GO) polyethyleneimine (PEI) film  
98 and anti-cystatin C antibody, without the use of redox probes during electrochemical measurements [32].  
99 The above mentioned methods were also used to detect hCC on synthetic plastic antibody for hCC designed  
100 with the molecularly imprinted polymer (MIP) technique on a carbon screen-printed electrode [33]. The  
101 EIS method was previously used for hCC detection only using the electrochemical immunosensor based on  
102 interdigitated electrode (IDE) modified with polypyrrole/carbon nanotube nanohybrid film and  
103 monoclonal antibodies anti-CysC [34].

104 However, to our knowledge, the EIS technique has not yet been suggested before for studies on  
105 interactions between hCC and membrane surface or protein-membrane interactions, exploiting a gold  
106 electrode. Nevertheless there are reports concerning the modification of gold electrodes for the purpose of  
107 detecting proteins in bacterial membrane extracts with the EIS and CV techniques [35]. Additionally, the  
108 interactions between amyloid  $\beta$  monomers ( $A\beta$ Ms) and amyloid  $\beta$  oligomers ( $A\beta$ Os) and a floating bilayer  
109 lipid membrane (fBLM) using gold electrodes were previously studied with EIS and IR spectroscopy  
110 techniques [36].

111 In this study a gold electrode modified with the 6-Mercaptohexan-1-ol (MCH) and DMPC  
112 membrane mimetic was applied for monitoring electrochemical changes resulting from the interaction  
113 between the functionalized electrode surface and V57G variant of hCC at concentrations ranging from  $1 \times$   
114  $10^{-14}$  M to  $1 \times 10^{-6}$ . The electrochemical changes were monitored with EIS and CV techniques. The CV  
115 results indicate that the most significant current changes were evident after incubation in a solution  
116 containing hCC V57G at the concentration of  $1 \times 10^{-14}$ . The EIS measurements confirmed the CV data. The  
117 most significant changes in charge transfer resistance were observed for the hCC V57G solution at the  
118 concentration of  $1 \times 10^{-14}$  M. The incubation of electrode in hCC V57G solutions at higher concentration  
119 caused insignificant changes observed in electrochemical impedance spectra. Additionally, the calculated  
120 surface coverage  $\theta_R$  confirmed that the electrode is coated in a similar manner for incubation studies in  
121 solutions at concentrations ranging from  $1 \times 10^{-12}$  M to  $1 \times 10^{-6}$  M. The modification of electrode surface  
122 and interactions between DMPC and hCC V57G were studied with the high-resolution X-ray photoelectron  
123 spectroscopy (XPS) and contact angle and surface free energy measurements.

## 124 **2. Methods and materials**

### 125 *2.1. Materials and reagents*

126 All solvents and reagents were used as received without further purification. 6-mercaptohexan-1-  
127 ol (MCH), 1,2-dimyristoyl-*sn*-glycero-3-phosphocholine (DMPC),  $K_3[Fe(CN)_6]$  and  $K_4[Fe(CN)_6]$  were  
128 purchased from Sigma-Aldrich.

### 129 *2.2. Expression and purification of human cystatin C*

130 The DNA of hCC V57G variant was obtained with site-directed mutagenesis as previously  
131 described [3]. Plasmid DNA (pHD313 vector [37]) including hCC gene coupled with signal peptide  
132 delivered from *E. coli* OmpA protein (responsible for secretion of hCC into the periplasmic space),  
133 temperature-sensitive  $\lambda$  cI 857 repressor,  $\lambda$  PR promoter and ampicillin resistance gene was expressed in *E.*  
134 *coli* BL21(DE3) competent cells according to earlier described-protocol [3].

### 135 2.3. DMPC phospholipid bilayer preparation

136 The lyophilized DMPC powder was suspended in PBS buffer (Sigma Aldrich). The phospholipid  
137 suspension was subjected to 15 incubation cycles involving 30 min incubation in ultrasound bath with  
138 heating (313 K) and 30 min incubation in 277 K. This procedure allowed to obtain stable, homogenous,  
139 and transparent solution of double-layered lipid bilayers. For the purpose of the experiment, 10 mM DMPC  
140 liposome stock solution was prepared and used for the preparation of a dilution series.

### 141 2.4. Functionalization of gold electrodes

142 The gold electrodes of 1.6 mm diameter used for all measurements were purchased from (Mineral,  
143 Poland). Before each modification, the electrodes were carefully polished using polishing pad saturated  
144 with micro polish alumina powder (1.0  $\mu\text{m}$ ; Buehler, USA). Then the electrodes were washed, dried in a  
145 stream of air, and placed in the vessel containing 1 mL of 1 mM MCH dissolved in absolute ethanol in  
146 order to obtain self-assembly monolayer on electrode surface. After 16 h the electrodes were washed with  
147 ethanol and dried. Afterwards, the electrode was modified with a layer of DMPC via incubation of its  
148 surface in 10  $\mu\text{L}$  of 1  $\mu\text{M}$  solution of DMPC for 1 h. The DMPC concentration used for electrode  
149 modification was higher than the critical micelle concentration (CMC) value (6nM), to ascertain the  
150 formation bilayer of DMPC on the electrode. The electrodes obtained in above manner were incubated in  
151 the hCC V57G solution at ascending concentrations ranging from  $1 \times 10^{-14}$  M to  $1 \times 10^{-6}$  M for 50 minutes.  
152 After each electrochemical measurement the electrodes were rinsed with a 0.01 M PBS solution, pH 7.4.

153 The gold electrodes of 11 mm x11 mm used in an XPS, contact angle and surface free energy  
154 experiments were purchased from (Arrandee, Germany). Before use the electrodes were incubated in a  
155 concentrated sulfuric acid for 4 minutes, washed with water and ethanol and modified according to the same  
156 procedure as described above for gold electrodes of 1.6 mm diameter.

### 157 2.5. X-ray photoelectron spectroscopy measurements

158 X-ray photoelectron spectroscopy (XPS) analyses were carried out using the Escalab 250Xi  
159 spectroscope (ThermoFisher Scientific) utilizing AlK $\alpha$  X-ray spot, diameter 500  $\mu\text{m}$ . The pass energy was  
160 set up to 20 eV. The low-energy electron and low-energy Ar<sup>+</sup> ion bombardment were used for charge  
161 compensation with final peak calibration using adventitious C1s (284.6 eV). Peak deconvolution was  
162 performed in Avantage v.59921 provided by spectroscope manufacturer.

### 163 2.6. Contact angle and surface free energy measurements

164 The Drop Shape Analyzer – DSA100 by Krüss was used to determine the contact angle and surface  
165 free energy of investigated samples. The contact angles of drops of four different liquids (water, formamide,



166 glycerol, and diiodomethane) were measured to determine the surface free energy. The image of a 4  $\mu$ L  
167 drop of the probe liquid deposited using a syringe was captured by a camera and after the digital image  
168 analysis, the average contact angle was deduced using the Young-Laplace method from the angles measured  
169 at both sides of the drop in equilibrium. The measurements were repeated 20 times. The total surface free  
170 energy  $\gamma_s$  and its dispersive  $\gamma_d$  and polar  $\gamma_p$  components of the surfaces were determined by the Owens,  
171 Wendt, Rabel, and Kaelble (OWRK) method from the contact angles of the three liquid drops (water,  
172 formamide and diiodomethane) [38–40].

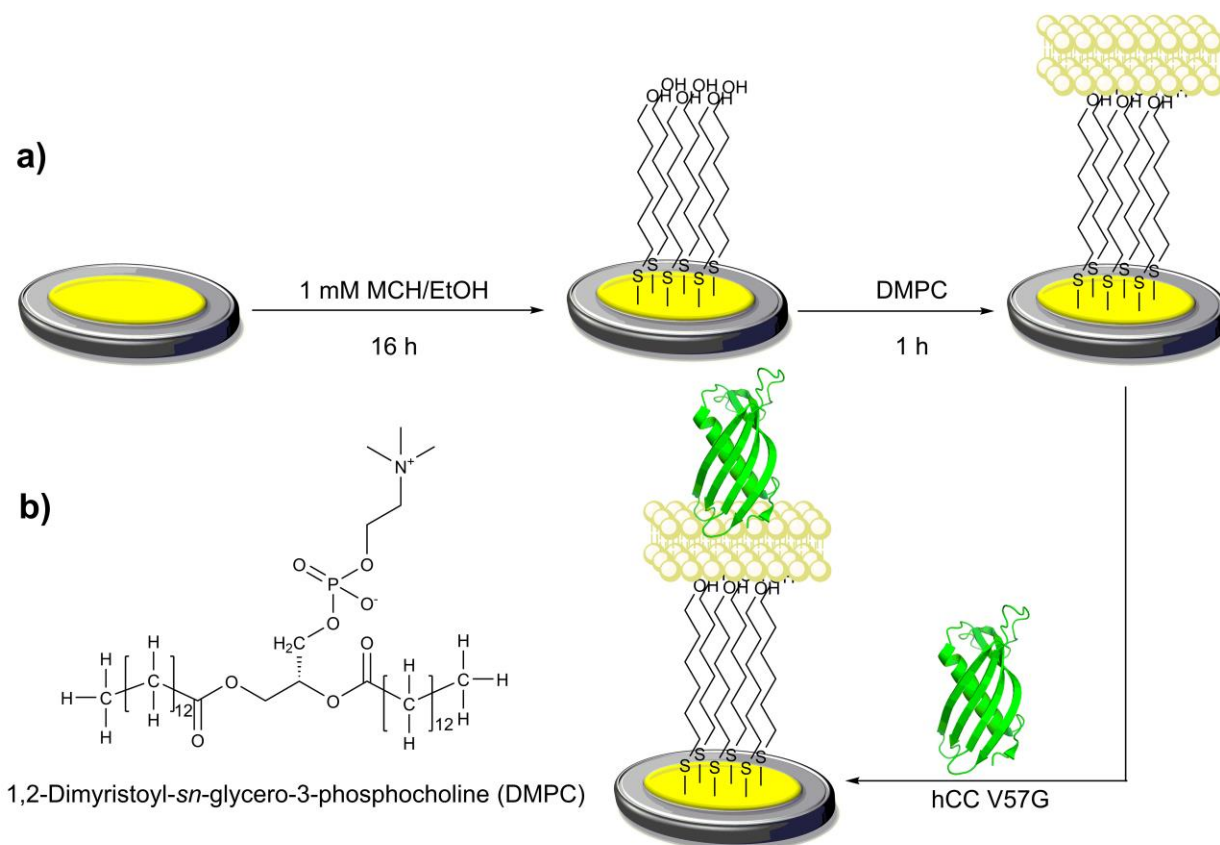
### 173 *2.7. Electrochemical impedance spectroscopy and cyclic voltammetry measurements*

174 The cyclic voltammetry (CV), and electrochemical impedance spectroscopy (EIS) measurements  
175 were performed using M204 multichannel potentiostat (Autolab, Netherlands) equipped with FRA32M  
176 electrochemical impedance spectroscopy module in a three-electrode cell. The unmodified and modified  
177 gold electrodes served as working electrodes, Ag/AgCl (0.1 M KCl) was a reference electrode and platinum  
178 wire was a counter electrode. All electrochemical measurements were performed in 0.01 M PBS solution  
179 of pH 7.0 containing  $\text{Fe}(\text{CN})_6^{3-/4-}$  as redox probes, containing 1 mM  $\text{K}_3[\text{Fe}(\text{CN})_6]$  and 1 mM  $\text{K}_4[\text{Fe}(\text{CN})_6]$   
180 (1 : 1). The cyclic voltammograms were obtained at scan rate of 0.1 V/s. The EIS spectra were obtained  
181 with frequency range of 0.1 Hz to 10 kHz, at with perturbation amplitude of 10 mV, at the open circuit  
182 potential (OCP). All the spectra were analyzed using ZSimpWin 3.21 impedance analysis software. All EIS  
183 spectra were fitted using modified Randles equivalent circuit  $R_s(Q(R_{ct}W))$ , where  $R_s$  is electrolyte  
184 resistance,  $Q_{dl}$  – constant phase element,  $R_{ct}$  – charge transfer resistance, and  $W$  – Warburg element.

185 **3. Results and discussion**

186 *3.1. The gold electrode modification procedure*

187 The gold electrodes used for detection of hCC V57G were modified according to the scheme shown  
188 in Figure 1a. The crystallographic structure of hCC V57G presented in Figure 1 was previously reported in  
189 [41]. In the first stage of the modification process MCH was applied to create a stable self-assembled  
190 monolayers (SAMs) on the gold electrode surface due to the fact that, it forms an organized layer on the  
191 electrode [42]. The SAMs formation is usually used in the first step of the process of electrode  
192 functionalization for construction of electrochemical sensors and biosensors [43–45]. In this work 1 mM  
193 ethanolic solution of MCH was used for electrode modification. The modification of gold electrodes with  
194 MCH takes place not only in ethanolic solution [46], but also in an aqueous solutions [47] or buffer solutions  
195 [48]. During the second stage the gold electrode was modified with DMPC by immersing electrode in 1  
196  $\mu$ M DMPC solution in PBS for 1 h. The chemical structure of the DMPC membrane is shown in Figure 1b.  
197 The electrode fabricated in this procedure was directly applied to measurements using CV and EIS methods.

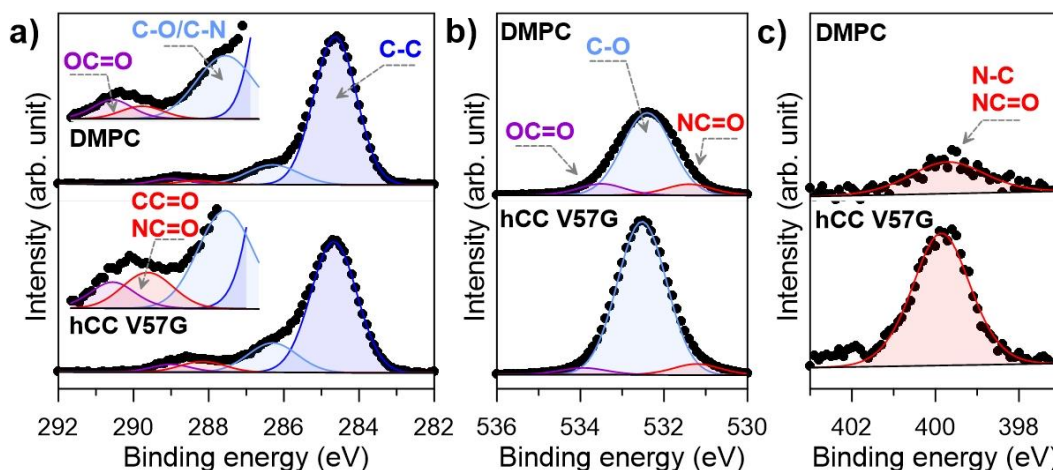


198 **Figure 1.** (a) The modification of gold electrode with MCH and DMPC for the hCC V57G detection. (b)  
199 The chemical structure of DMPC.  
200



201 3.2. XPS Measurements

202 The XPS spectra were registered to analyze Au electrode surface chemistry and confirm the  
203 successful anchoring of hCC V57G to the DMPC-functionalized surface. The results of XPS analysis for  
204 primary film constituents are presented in Figure 2.



205  
206 **Figure 2.** High-resolution XPS measurements of the electrode surface after DMPC and hCC  
207 functionalization steps, studied in the core-level binding energy range of (a) C1s, six times enhanced in the  
208 inset, (b) O1s, and (c) N1s with proposed deconvolution model.

209 The dominant component of the C1s spectra (Figure 2a) is C-C aliphatic bond (284.6 eV) within  
210 the DMPC and hCC V57G. Furthermore, three additional components can be distinguished, representing  
211 different oxidized forms of organic carbon. Their peak positions are characteristic for C-O and C-N  
212 interactions (286.3 eV), aliphatic esters, carbonyls, amides, imides (288.3 eV), and carboxyl groups (289.0  
213 eV). The share of all oxidized species in total [C] equals 18.0 % in case of DMPC and increases  
214 significantly, reaching even 27.3 % after hCC V57G anchoring. Here, the share of the C=O/NC=O moieties  
215 increases the most, from 2.8 up to 5.9 % of total [C]. Unfortunately, the signals representing single  
216 phosphorus atoms from within DMPC structure or S atom present in the thiol groups were too low for the  
217 threshold of the spectroscope and were not detected. The detailed deconvolution analysis is presented in  
218 Table 1.

219  
220  
221  
222

223 **Table 1.** Results of XPS data deconvolution (in at.%).

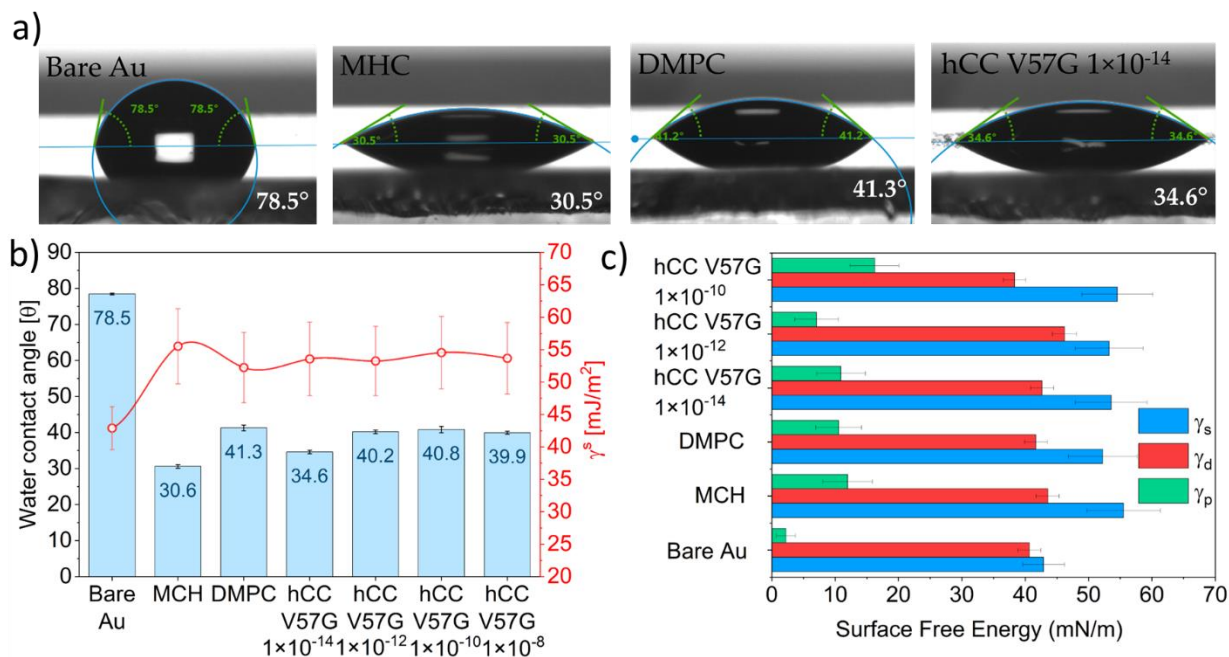
	C1s					O1s		N1s
	C-C	C-O	C=O/ NC=O	OC=O	NC=O	C-O	OC=O	N-C/ NC=O
BE (eV)	284.6	286.3	288.2	289.0	531.2	532.5	533.9	399.9
DMPC	46.1	7.5	1.6	1.1	33.9	4.6	4.5	0.7
hCC V57G	24.7	5.9	1.3	2.0	57.5	4.2	2.5	1.9

224

225 The above-mentioned observations are assisted by a tremendous rise in oxygen content, analyzed  
 226 based on the O1s spectra (Figure 2b). The total share of all [O] species increases from 43.0 up to 64.21  
 227 at.%, when  $C_{580}H_{910}N_{170}O_{176}S_7$  (hCC V57G) is anchored to the modified electrode surface. The surface  
 228 modification with hCC V57G particularly affects the C-O bonds (O1s at 532.5 eV), which corroborate with  
 229 the findings observed from the C1s peak analysis. Moreover, over two-fold increase in the N1s share, from  
 230 0.7 to 1.9 at.% was also observed. The N1s peak used for the deconvolution is located at 399.9 eV, a value  
 231 characteristic for amide or imides but also amines.

### 232 3.3. Contact angle and surface free energy measurements

233 Wettability measurements at the modified gold electrode surface allowed to determine the influence  
 234 of the modification process on the characteristics of the tested systems (Figure 3). The obtained results  
 235 clearly indicate that the modification of the gold electrode with MCH causes a significant change in its  
 236 properties. The decrease in the contact angle from  $78.5^\circ$  for the bare electrode to  $30.6^\circ$  for the 1-hexanethiol-  
 237 modified surface is a significant change. The presence of MCH made the surface more hydrophilic, which  
 238 is the result of the presence of -OH groups on the modified electrode surface. The introduction of the DMPC  
 239 membrane into the system, in turn, causes an increase in hydrophobicity, which is manifested in an increase  
 240 in the contact angle to  $41.3^\circ$  (Figure 3a). Further studies showed that the interaction with hCC V57G is  
 241 visible for the concentration of  $10^{-14}$  M. For electrodes incubated in such protein concentration, we observe  
 242 a decrease in hydrophobicity by approx.  $7^\circ$  compared to electrodes with a DMPC membrane. In turn, the  
 243 electrodes incubated in higher hCC V57G concentrations showed only slight changes in the contact angle  
 244 (approx.  $1-2^\circ$ ). This clearly indicates that the electrode is sensitive only below the concentration of  $1 \times 10^{-14}$   
 245 M.



246

247

248 **Figure 3.** (a) Wettability measurement photos, (b) water contact angle and surface free energy  
 249  $\gamma^s$  (red line), and (c) surface free energy  $\gamma_s$  diagram (blue bar) with disperse (red bar) and polar (green bar)  
 250 parts, for each step of the modification of the gold electrode for hCC V57G sensing.

251 Surface free energy allows to determine the biocompatibility of a given system, as well as to track  
 252 the interactions or physicochemical changes resulting from the interactions of the system with the analyte.  
 253 The modification of the gold electrode with a thiol layer increases the surface free energy (around 15 mN/m)  
 254 (Figure 3b,c). This is due to a significant increase in the share of the polar part (Figure 3c), resulting from  
 255 the appearance of functional groups on the surface of the electrode, which were not present in the case of a  
 256 bare electrode. Further anchoring of the DMPC membrane on the thiol surface reduces the free energy, but  
 257 only by about 5 mN/m (Figure 3c). Such an effect may be caused by the arrangement of the lipid bilayer  
 258 formed by DMPC. Changes in the contact angle and surface free energy (Figure 3b) indicate that the  
 259 membrane surface has hydrophilic heads pointing outward from the layer. Hence, the hydrophilic character  
 260 of the system is maintained, although it is weaker compared to the thiol layer rich in -OH groups. In the  
 261 case of surface free energy parameters, we do not observe such a large variability in the presence of  
 262 interaction with hCC V57G as in the case of the contact angle value. Nevertheless, the share of both  
 263 dispersive and polar interactions (hydrogen bonding and dipole-dipole interactions) is visible.

264

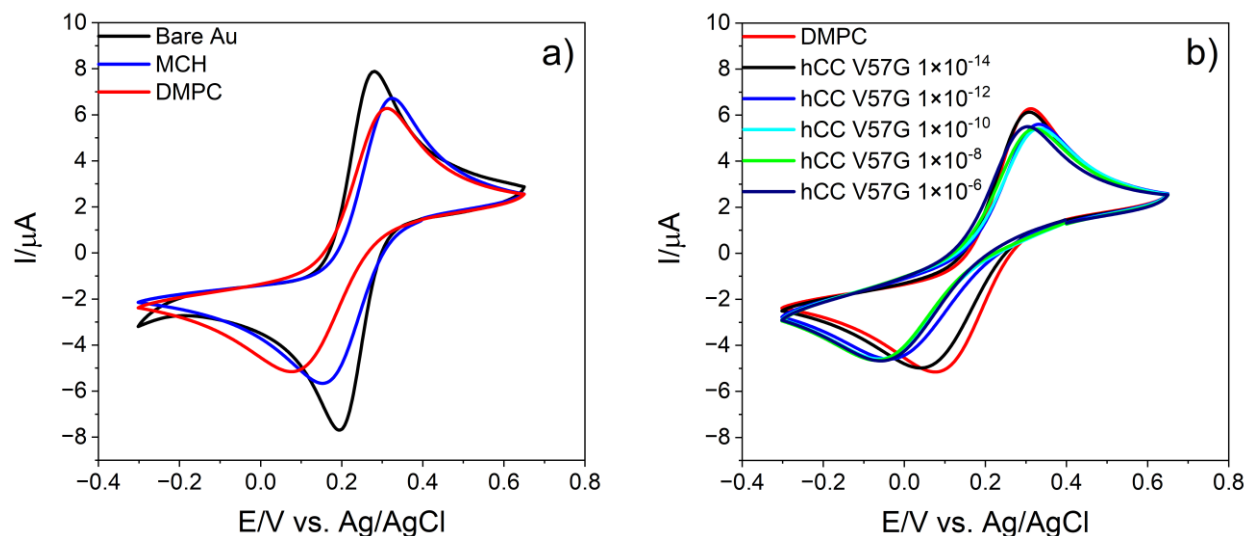
265



## 266 3.4. Electrochemical measurements

### 267 3.4.1. Cyclic voltammetry (CV)

268 The cyclic voltammetry (CV) was used to characterize the response of an electrode during the  
269 modification steps and in order to examine the electrode after incubation in hCC V57G solutions at  
270 concentrations ranging from  $1 \times 10^{-14}$  M to  $1 \times 10^{-6}$  M. Figure 4a shows the cyclic voltammograms obtained  
271 for bare gold electrode before and after modification with MCH and DMPC. All measurements were  
272 performed in 0.01 M PBS solution (pH 7.0) containing 1 mM  $\text{Fe}(\text{CN})_6^{3-/4-}$  used as redox probe. The two  
273 reversible peaks are observed on cyclic voltammograms with peak-to-peak separation ( $\Delta E$ ) of 76 mV. The  
274 intensity current of peaks decrease after modification with MCH with the peak-to-peak separation  
275 increasing to 159 mV, suggesting the SAMs formation on the electrode surface. Similar value of ( $\Delta E$ ) was  
276 observed in the previous paper indicating the formation of monolayer on a gold electrode [49]. Further  
277 functionalization of the electrode with DMPC leads to an even greater decrease in current intensity and an  
278 increase in peak-to-peak separation to 214 mV. The above-mentioned changes indicate that electron transfer  
279 to the surface of the electrode has been inhibited, indicating that its surface has been modified. The cyclic  
280 voltammograms of the modified electrode after incubation in PBS solution containing different  
281 concentrations of hCC V57G are shown in Figure 4b. The incubation in  $1 \times 10^{-14}$  M hCC V57G solution  
282 causes a slight decrease in anodic peak and a shift in the position of the cathodic peak, with peak-to-peak  
283 separation ( $\Delta E$ ) of 250 mV relative to the voltammogram observed for DMPC. The changes observed in  
284 the cyclic voltammograms for hCC V57G at the concentration of  $1 \times 10^{-14}$  M are most significant. Further  
285 incubation in a solution containing  $1 \times 10^{-12}$  M hCC V57G solution causes further decrease in the current  
286 intensity and an increase of ( $\Delta E$ ) to 311 mV. At the same time, after incubation in hCC V57G solutions at  
287 the concentration of  $1 \times 10^{-10}$  M and  $1 \times 10^{-8}$  M, almost identical voltammograms were obtained with  $\Delta E$   
288 of 362 mV and 359 mV respectively. The incubation in  $1 \times 10^{-6}$  M hCC V57G solution also does not cause  
289 changes in the peak heights, only a shift of the anode peak towards negative values is observable resulting  
290 in  $\Delta E$  decrease to 329 mV. The CV analysis indicates that the most significant changes are observed after  
291 incubation of the electrode in  $1 \times 10^{-14}$  M hCC V57G solution.



292  
 293 **Figure 4.** (a) Cyclic voltammograms of bare Au electrode and electrodes modified with MCH and DMPC.  
 294 (b) Cyclic voltammograms of the DMPC-modified electrode after incubation in hCC V57G solutions at  
 295 concentrations ranging from  $1 \times 10^{-14}$  M to  $1 \times 10^{-6}$  M recorded in 0.01 M PBS (pH 7.0) containing 1 mM  
 296  $\text{Fe}(\text{CN})_6^{3-/4-}$ , scan rate 100 mV/s.

### 297 3.4.2. Electrochemical Impedance Spectroscopy (EIS)

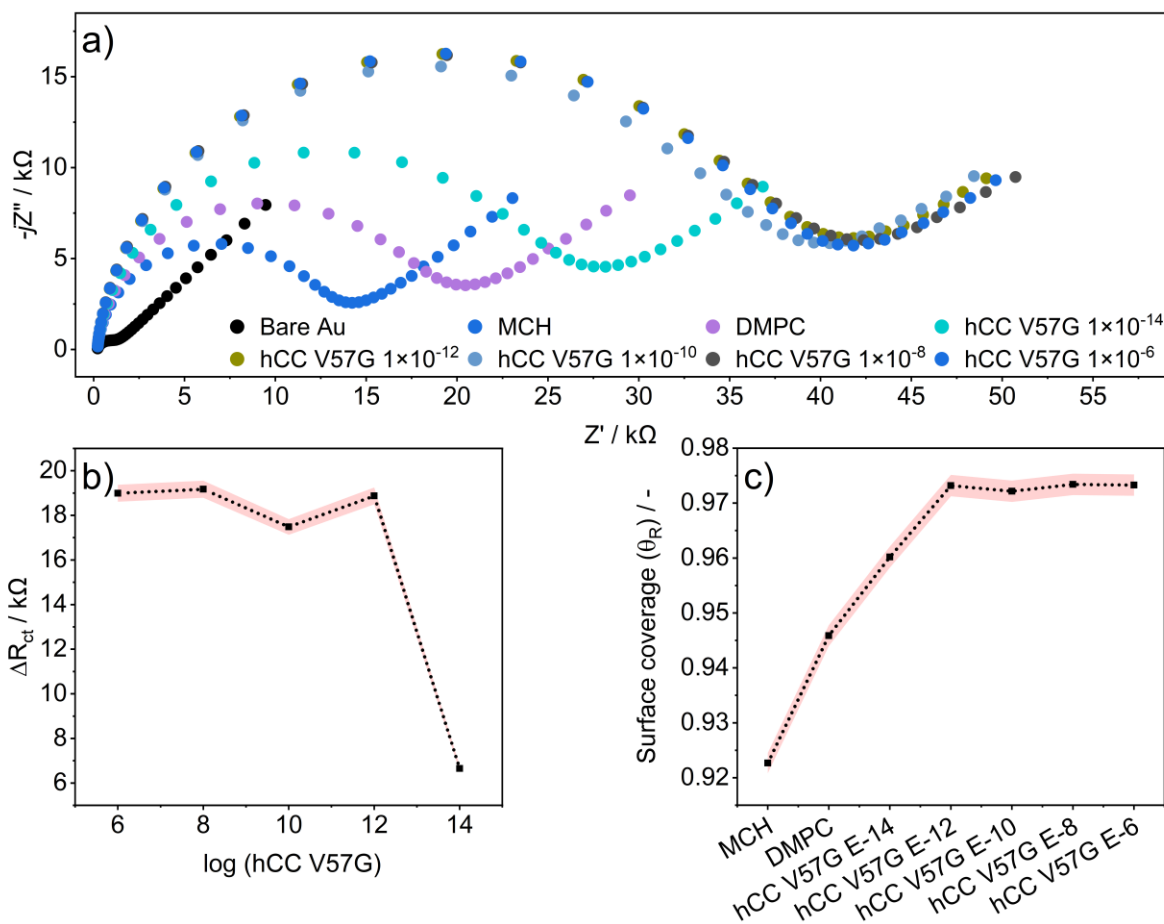
298 The EIS measurements were performed in 0.01 M PBS solution (pH 7.0) containing  $\text{Fe}(\text{CN})_6^{3-/4-}$ .  
 299 Figure 5a shows the impedance spectra obtained for bare Au electrode, electrode modified with MCH,  
 300 electrode modified with DMPC and the modified electrodes after incubation in hCC V57G solutions at  
 301 concentrations ranging from  $1 \times 10^{-14}$  M to  $1 \times 10^{-6}$  M. All spectra were fitted using modified Randles  
 302 equivalent circuit  $R_s(Q_{dl}(R_{ct}W))$ . The charge transfer resistance calculated for a bare electrode ( $R_{ct} = 1.003$   
 303  $\text{k}\Omega$ ) increases significantly after modification with MCH to ( $R_{ct} = 12.970 \text{ k}\Omega$ ) with the decreases of constant  
 304 phase element ( $Q_{dl}$ ) from  $1.426 \mu\text{F}$  for bare Au electrode to  $0.191 \mu\text{F}$  after MCH modification. A similar  
 305 phenomenon was also observed in previous work [49]. The Au electrode coated with MCH additionally  
 306 modified with DMPC causes an increase of  $R_{ct}$  to  $18.530 \text{ k}\Omega$  and increase of constant phase element ( $Q_{dl}$ )  
 307 to  $0.212 \mu\text{F}$  (see Table S1 in Supplementary Information). Further incubation in hCC V57G solutions at  
 308 the concentrations of  $1 \times 10^{-14}$  M cause an increase of the charge transfer resistance  $R_{ct}$  to  $25.180 \text{ k}\Omega$ . A  
 309 subsequent incubation in hCC V57G solutions at higher concentrations causes an increase of  $R_{ct}$  to  $37.400$   
 310  $\text{k}\Omega$  after incubation in  $1 \times 10^{-12}$  M hCC V57G and remains constant ( $37.520 \text{ k}\Omega$ ) for  $1 \times 10^{-6}$  M hCC V57G  
 311 solution. It's also worth noting that after DMPC modification the parameter  $n$  is constant regardless of any  
 312 incubation in hCC V57G solution and is close to 1 [36]. This indicates that the surface roughness does not  
 313 change significantly during subsequent stages of hCC V57G detection at different concentrations [50]. The  
 314 understanding of the mechanism of interactions between the DMPC layer immobilized on the gold electrode

315 and hCC V57G at different concentrations requires additional research. Nevertheless, the previous EIS  
316 studies on interaction between amyloid  $\beta$  monomers ( $A\beta$ Ms) and the floating bilayer lipid membrane  
317 (fBLM) do not lead to the formation of pores. Only the  $\beta$  oligomers ( $A\beta$ Os) induced the pore formation in  
318 examined membrane [36].

319 Figure 5b shows the  $\Delta R_{ct}$  correlation, where  $\Delta R_{ct}$  was calculated as difference between the  $R_{ct}$  after  
320 electrode incubation in hCC V57G solutions of different concentration and  $R_{ct}$  of DMPC and the logarithm  
321 of the hCC V57G concentration. The above relationship clearly shows that the calculated change in  $\Delta R_{ct}$   
322 for the electrode after incubation in  $1 \times 10^{-14}$  M hCC V57G solution reaches a value of 6.650 k $\Omega$ , then  
323 rapidly increases to 18.870 k $\Omega$  after incubation in  $1 \times 10^{-12}$  M hCC V57G solution. Subsequent incubations  
324 in higher concentrations of hCC V57G result in only slight changes in  $\Delta R_{ct}$  values, suggesting that the  
325 resulting electrode is not so sensitive to the presence of hCC V57G at the higher concentrations ranging  
326 from  $1 \times 10^{-12}$  M to  $1 \times 10^{-6}$  M.

327 Figure 5c shows the plot of surface coverage  $\theta_R$  after each step of bare Au modification, calculated  
328 according to the following equation  $\theta_R = 1 - (R_{ct}(\text{Bare Au}) / R_{ct}(\text{Modified Au}))$  [51,52], where  $R_{ct}(\text{Bare Au})$  and  $R_{ct}$   
329  $(\text{Modified Au})$  corresponds to the charge transfer resistance for the bare electrode and the appropriately modified  
330 electrodes respectively. The surface coverage of gold electrode after SAMs formation was 0.923, while  
331 after DMPC modification the surface coverage increased to 0.946, then after incubation in hCC V57G  
332 solution at the concentration of  $1 \times 10^{-14}$  M the surface coverage was 0.960. The incubations of the modified  
333 gold electrode in hCC V57G solution with concentrations ranging from  $1 \times 10^{-12}$  M to  $1 \times 10^{-6}$  M did not  
334 change the electrode coverage. The calculated surface coverage value for each electrode was constant at  
335 0.973. The 0.97 degree coverage of the electrode surface may indicate that pores can be present on the  
336 bilayer of DMPC deposited on the electrode, which allows the redox probe to reach the electrode. This  
337 unequivocally proves that the gold electrode used in this study shows the most significant changes after  
338 incubation in the solution of hCC V57G at concentration of  $1 \times 10^{-14}$  M. The lack of significant changes  
339 above the concentrations of  $10^{-14}$  M of hCC V57G can be attributed to the saturation of binding sites on the  
340 electrode surface. The previously published data shows that only an external random coil loop region of  
341 hCC protein interacts with DMPC bilayer and the protein does not migrate into the bilayer, but interacts  
342 with its surface [15].

343



344

345 **Figure 5.** The electrochemical impedance spectra obtained for (a) bare Au electrode, electrodes modified  
 346 with MCH and DMPC and modified electrodes after incubation in hCC V57G solutions at concentrations  
 347 ranging from  $1 \times 10^{-14}$  M to  $1 \times 10^{-6}$  M. (b) Correlation between  $\Delta R_{ct}$  and the logarithm of the hCC V57G  
 348 concentration. (c) The electrode surface coverage after each step of modification. The red lines indicate the  
 349 error bars.

350 CV and EIS technique have not been applied before for studies on interactions between hCC and  
 351 membrane surface or protein-membrane interactions with the use of gold electrodes. The presented studies  
 352 proves that the CV and EIS methods can be applied for the monitoring of changes occurring on the surface  
 353 of an electrode modified with the DMPC bilayer during incubation in the V57G solution at different  
 354 concentrations. EIS measurements also indicate that the hCC V57G can be detected at the concentrations  
 355 ranging from  $1 \times 10^{-14}$  M to  $1 \times 10^{-6}$  M, nevertheless the most significant changes were observed for the  
 356 hCC V57G at the concentration of  $1 \times 10^{-14}$  M.

357

358



#### 359 4. Conclusion

360 The presented research indicates that the gold electrode modified with MCH and DMPC bilayer,  
361 allows for monitoring the interactions between DMPC and V57G mutant of human cystatin C. The  
362 interactions between the modified electrode and the hCC V57G protein were monitored at concentrations  
363 ranging from  $1 \times 10^{-14}$  M to  $1 \times 10^{-6}$  M. Both the CV and EIS measurements indicate that the most significant  
364 changes were observed for the protein detection at the concentration of  $1 \times 10^{-14}$  M. The incubation in hCC  
365 V57G solutions at higher concentration did not cause any changes relevant in the experimental conditions.  
366 Furthermore, the EIS measurements indicate that incubation of the modified electrode in hCC V57G  
367 solutions, at concentrations ranging from  $1 \times 10^{-12}$  M to  $1 \times 10^{-6}$  M, did not change the electrode coverage.  
368 The electrochemical data obtained in this study were also confirmed with water contact angle and surface  
369 free energy measurements. The decrease in contact angle upon MCH modification highlights the  
370 enhancement of surface hydrophilicity, while the subsequent increase in contact angle after the addition of  
371 the DMPC membrane signifies the increase of hydrophobicity of the modified surface. The sensitivity of  
372 the electrode in relation to the interaction with hCC V57G at different concentrations was reflected in the  
373 contact angle measurements. The most noticeable decrease in hydrophobicity (by approximately  $7^\circ$ ) was  
374 observed for electrodes incubated with hCC V57G at the concentration of  $10^{-14}$  M. Obtained results confirm  
375 that the presented method of electrode functionalization allows to monitor the interactions between the  
376 electrode surface and hCC V57G protein.

377

#### 378 Declaration of interests

379 The authors declare that they have no known competing financial interests or personal relationships that  
380 could have appeared to influence the work reported in this paper.

381

#### 382 Acknowledgements

383 This work was financially supported by Harmonia 10 grant (2018/30/M/ST4/00039) from National Science  
384 Centre, Poland. We thank Prof. Artur Zieliński and Prof. Robert Szoszkiewicz for scientific discussions  
385 and Weronika Janik for technical support.

386

387

388



389 **6. Reference**

- 390 [1] M.D. Benson, J.N. Buxbaum, D.S. Eisenberg, G. Merlini, M.J.M. Saraiva, Y. Sekijima, J.D. Sipe, P.  
391 Westermark, Amyloid nomenclature 2018: recommendations by the International Society of  
392 Amyloidosis (ISA) nomenclature committee, *Amyloid*, 25 (2018) 215–219.
- 393 [2] M.D. Benson, J.N. Buxbaum, D.S. Eisenberg, G. Merlini, M.J.M. Saraiva, Y. Sekijima, J.D. Sipe, P.  
394 Westermark, Amyloid nomenclature 2020: update and recommendations by the International Society  
395 of Amyloidosis (ISA) nomenclature committee, *Amyloid*, 27 (2020) 217–222.
- 396 [3] A. Szymańska, A. Radulska, P. Czaplewska, A. Grubb, Z. Grzonka, S. Rodziewicz-Motowidło,  
397 Governing the monomer-dimer ratio of human cystatin c by single amino acid substitution in the  
398 hinge region, *Acta Biochim. Pol.*, 56 (2009).
- 399 [4] A. Onopiuk, A. Tokarzewicz, E. Gorodkiewicz, Cystatin C: a kidney function biomarker, *Adv. Clin.*  
400 *Chem.*, 68 (2015) 57–69.
- 401 [5] M. Abrahamson, A.J. Barrett, G. Salvesen, A. Grubb, Isolation of six cysteine proteinase inhibitors  
402 from human urine Their physicochemical and enzyme kinetic properties and concentrations in  
403 biological fluids, *J. Biol. Chem.*, 261 (1986) 11282–11289.
- 404 [6] I. Ekiel, M. Abrahamson, Folding-related Dimerization of Human Cystatin C (\*), *J. Biol. Chem.*, 271  
405 (1996) 1314–1321.
- 406 [7] M.F.M. Sciacca, C. Tempra, F. Scollo, D. Milardi, C. La Rosa, Amyloid growth and membrane  
407 damage: Current themes and emerging perspectives from theory and experiments on A $\beta$  and hIAPP,  
408 *Biochim. Biophys. Acta BBA - Biomembr.*, 1860 (2018) 1625–1638.
- 409 [8] A. Vahdat shariat panahi, P. Hultman, K. Öllinger, G.T. Westermark, K. Lundmark, Lipid membranes  
410 accelerate amyloid formation in the mouse model of AA amyloidosis, *Amyloid*, 26 (2019) 34–44.
- 411 [9] M.S. Terakawa, Y. Lin, M. Kinoshita, S. Kanemura, D. Itoh, T. Sugiki, M. Okumura, A.  
412 Ramamoorthy, Y.-H. Lee, Impact of membrane curvature on amyloid aggregation, *Biochim. Biophys.*  
413 *Acta BBA - Biomembr.*, 1860 (2018) 1741–1764.
- 414 [10] S.M. Butterfield, H.A. Lashuel, Amyloidogenic Protein–Membrane Interactions: Mechanistic Insight  
415 from Model Systems, *Angew. Chem. Int. Ed.*, 49 (2010) 5628–5654.
- 416 [11] J.D. Harper, S.S. Wong, C.M. Lieber, P.T. Lansbury, Observation of metastable A $\beta$  amyloid  
417 protofibrils by atomic force microscopy, *Chem. Biol.*, 4 (1997) 119–125.
- 418 [12] C. Ionescu-Zanetti, R. Khurana, J.R. Gillespie, J.S. Petrick, L.C. Trabachino, L.J. Minert, S.A. Carter,  
419 A.L. Fink, Monitoring the assembly of Ig light-chain amyloid fibrils by atomic force microscopy,  
420 *Proc. Natl. Acad. Sci.*, 96 (1999) 13175–13179.
- 421 [13] M. Wahlbom, X. Wang, V. Lindström, E. Carlemalm, M. Jaskolski, A. Grubb, Fibrillogenic  
422 Oligomers of Human Cystatin C Are Formed by Propagated Domain Swapping\*, *J. Biol. Chem.*, 282  
423 (2007) 18318–18326.
- 424 [14] P. Jurczak, E. Sikorska, P. Czaplewska, S. Rodziewicz-Motowidło, I. Zhukov, A. Szymanska, The  
425 Influence of the Mixed DPC:SDS Micelle on the Structure and Oligomerization Process of the Human  
426 Cystatin C, *Membranes*, 11 (2021) 17.
- 427 [15] P. Jurczak, K. Szutkowski, S. Lach, S. Jurga, P. Czaplewska, A. Szymanska, I. Zhukov, DMPC  
428 Phospholipid Bilayer as a Potential Interface for Human Cystatin C Oligomerization: Analysis of  
429 Protein-Liposome Interactions Using NMR Spectroscopy, *Membranes*, 11 (2021) 13.
- 430 [16] M. Beseničar, P. Maček, J.H. Lakey, G. Anderluh, Surface plasmon resonance in protein–membrane  
431 interactions, *Chem. Phys. Lipids*, 141 (2006) 169–178.
- 432 [17] M.J. Swamy, R.S. Sankhala, B.P. Singh, Thermodynamic Analysis of Protein–Lipid Interactions by  
433 Isothermal Titration Calorimetry, in: J.H. Kleinschmidt (Ed.), *Lipid-Protein Interact. Methods*  
434 *Protoc.*, Springer, New York, NY, 2019: pp. 71–89.
- 435 [18] S.A. Tatulian, FTIR Analysis of Proteins and Protein–Membrane Interactions, in: J.H. Kleinschmidt  
436 (Ed.), *Lipid-Protein Interact. Methods Protoc.*, Springer, New York, NY, 2019: pp. 281–325.

- 437 [19] O. Vadas, M.L. Jenkins, G.L. Dornan, J.E. Burke, Chapter Seven - Using Hydrogen–Deuterium  
 438 Exchange Mass Spectrometry to Examine Protein–Membrane Interactions, in: M.H. Gelb (Ed.),  
 439 *Methods Enzymol.*, Academic Press, 2017: pp. 143–172.
- 440 [20] E.E. Scott, C.R. Wolf, M. Otyepka, S.C. Humphreys, J.R. Reed, C.J. Henderson, L.A. McLaughlin,  
 441 M. Paloncyova, V. Navratilova, K. Berka, P. Anzenbacher, U.P. Dahal, C. Barnaba, J.A. Brozik, J.P.  
 442 Jones, F. Estrada, J.S. Laurence, J.W. Park, W.L. Backes, The Role of Protein-Protein and Protein-  
 443 Membrane Interactions on P450 Function, *Drug Metab. Dispos.*, (2016).
- 444 [21] S.B. Nielsen, D.E. Otzen, Quartz Crystal Microbalances as Tools for Probing Protein–Membrane  
 445 Interactions, in: J.H. Kleinschmidt (Ed.), *Lipid-Protein Interact. Methods Protoc.*, Springer, New  
 446 York, NY, 2019: pp. 31–52.
- 447 [22] C. Aisenbrey, M. Michalek, E.S. Salnikov, B. Bechinger, Solid-State NMR Approaches to Study  
 448 Protein Structure and Protein–Lipid Interactions, in: J.H. Kleinschmidt (Ed.), *Lipid-Protein Interact.*  
 449 *Methods Protoc.*, Humana Press, Totowa, NJ, 2013: pp. 357–387.
- 450 [23] R.A.S. Smith, A. Nabok, B.J.F. Blakeman, W.-F. Xue, B. Abell, D.P. Smith, Analysis of Toxic  
 451 Amyloid Fibril Interactions at Natively Derived Membranes by Ellipsometry, *PLOS ONE*, 10 (2015)  
 452 e0132309.
- 453 [24] D.J. Lindberg, E. Wesén, J. Björkeröth, S. Rocha, E.K. Esbjörner, Lipid membranes catalyse the fibril  
 454 formation of the amyloid- $\beta$  (1–42) peptide through lipid-fibril interactions that reinforce secondary  
 455 pathways, *Biochim. Biophys. Acta BBA - Biomembr.*, 1859 (2017) 1921–1929.
- 456 [25] K. Sasahara, K. Morigaki, K. Shinya, Amyloid aggregation and deposition of human islet amyloid  
 457 polypeptide at membrane interfaces, *FEBS J.*, 281 (2014) 2597–2612.
- 458 [26] L.L. Martin, C. Kubeil, S. Piantavigna, T. Tikkoo, N.P. Gray, T. John, A.N. Calabrese, Y. Liu, Y.  
 459 Hong, M.A. Hossain, N. Patil, B. Abel, R. Hoffmann, J.H. Bowie, J.A. Carver, Amyloid aggregation  
 460 and membrane activity of the antimicrobial peptide uperin 35, *Pept. Sci.*, 110 (2018) e24052.
- 461 [27] X. Dong, Q. Qiao, Z. Qian, G. Wei, Recent computational studies of membrane interaction and  
 462 disruption of human islet amyloid polypeptide: Monomers, oligomers and protofibrils, *Biochim.*  
 463 *Biophys. Acta BBA - Biomembr.*, 1860 (2018) 1826–1839.
- 464 [28] Z. Lv, M. Hashemi, S. Banerjee, K. Zagorski, J.-C. Rochet, Y.L. Lyubchenko, Assembly of  $\alpha$ -  
 465 synuclein aggregates on phospholipid bilayers, *Biochim. Biophys. Acta BBA - Proteins Proteomics*,  
 466 1867 (2019) 802–812.
- 467 [29] A. Quist, I. Doudevski, H. Lin, R. Azimova, D. Ng, B. Frangione, B. Kagan, J. Ghiso, R. Lal, Amyloid  
 468 ion channels: A common structural link for protein-misfolding disease, *Proc. Natl. Acad. Sci.*, 102  
 469 (2005) 10427–10432.
- 470 [30] D. Desai, A. Kumar, D. Bose, M. Datta, Ultrasensitive sensor for detection of early stage chronic  
 471 kidney disease in human, *Biosens. Bioelectron.*, 105 (2018) 90–94.
- 472 [31] K.S.S. Devi, U.M. Krishnan, Microfluidic electrochemical immunosensor for the determination of  
 473 cystatin C in human serum, *Microchim. Acta*, 187 (2020) 585.
- 474 [32] E.K.G. Trindade, B.V.M. Silva, R.F. Dutra, A probeless and label-free electrochemical  
 475 immunosensor for cystatin C detection based on ferrocene functionalized-graphene platform, *Biosens.*  
 476 *Bioelectron.*, 138 (2019) 111311.
- 477 [33] R.S. Gomes, B.A. Gomez-Rodríguez, R. Fernandes, M.G.F. Sales, F.T.C. Moreira, R.F. Dutra, Plastic  
 478 Antibody of Polypyrrole/Multiwall Carbon Nanotubes on Screen-Printed Electrodes for Cystatin C  
 479 Detection, *Biosensors*, 11 (2021) 175.
- 480 [34] P.A.B. Ferreira, M.C.M. Araujo, C.M. Prado, R.A. de Lima, B.A.G. Rodríguez, R.F. Dutra, An  
 481 ultrasensitive Cystatin C renal failure immunosensor based on a PPy/CNT electrochemical capacitor  
 482 grafted on interdigitated electrode, *Colloids Surf. B Biointerfaces*, 189 (2020) 110834.
- 483 [35] L.J.C. Jeuken, S.D. Connell, M. Nurnabi, J. O’Reilly, P.J.F. Henderson, S.D. Evans, R.J. Bushby,  
 484 Direct Electrochemical Interaction between a Modified Gold Electrode and a Bacterial Membrane  
 485 Extract, *Langmuir*, 21 (2005) 1481–1488.



- 486 [36] D. Mrdenovic, Z. Su, W. Kutner, J. Lipkowski, P. Pieta, Alzheimer's disease-related amyloid  $\beta$   
487 peptide causes structural disordering of lipids and changes the electric properties of a floating bilayer  
488 lipid membrane, *Nanoscale Adv.*, 2 (2020) 3467–3480.
- 489 [37] M. Abrahamson, H. Dalbøge, I. Olafsson, S. Carlsen, A. Grubb, Efficient production of native,  
490 biologically active human cystatin C by *Escherichia coli*, *FEBS Lett.*, 236 (1988) 14–18.
- 491 [38] J. Kloubek, Development of methods for surface free energy determination using contact angles of  
492 liquids on solids, *Adv. Colloid Interface Sci.*, 38 (1992) 99–142.
- 493 [39] D.K. Owens, R.C. Wendt, Estimation of the surface free energy of polymers, *J. Appl. Polym. Sci.*, 13  
494 (1969) 1741–1747.
- 495 [40] A. Cirocka, D. Zarzeczańska, A. Wcisło, J. Ryl, R. Bogdanowicz, B. Finke, T. Ossowski, Tuning of  
496 the electrochemical properties of transparent fluorine-doped tin oxide electrodes by microwave  
497 pulsed-plasma polymerized allylamine, *Electrochimica Acta*, 313 (2019) 432–440.
- 498 [41] M. Maszota-Zieleniak, P. Jurczak, M. Orlikowska, I. Zhukov, D. Borek, Z. Otwinowski, P. Skowron,  
499 Z. Pietralik, M. Kozak, A. Szymańska, S. Rodziewicz-Motowidło, NMR and crystallographic  
500 structural studies of the extremely stable monomeric variant of human cystatin C with single amino  
501 acid substitution, *FEBS J.*, 287 (2020) 361–376.
- 502 [42] X. Xu, A. Makaraviciute, S. Kumar, C. Wen, M. Sjödin, E. Abdurakhmanov, U.H. Danielson, L.  
503 Nyholm, Z. Zhang, Structural Changes of Mercaptohexanol Self-Assembled Monolayers on Gold and  
504 Their Influence on Impedimetric Aptamer Sensors, *Anal. Chem.*, 91 (2019) 14697–14704.
- 505 [43] T. Swebocki, P. Niedziałkowski, A. Cirocka, E. Szczepańska, T. Ossowski, A. Wcisło, In pursuit of  
506 key features for constructing electrochemical biosensors – electrochemical and acid-base  
507 characteristic of self-assembled monolayers on gold, *Supramol. Chem.*, 32 (2020) 256–266.
- 508 [44] G. Chen, W. Chen, L. Xu, H. Jin, W. Sun, J. Lan, F. Wu, X. Zhang, J. Zhang, J. Chen, Sensitive,  
509 Highly Stable, and Anti-Fouling Electrode with Hexanethiol and Poly-A Modification for Exosomal  
510 microRNA Detection, *Anal. Chem.*, 94 (2022) 5382–5391.
- 511 [45] P. Niedziałkowski, M. Bojko, J. Ryl, A. Wcisło, M. Spodzieja, K. Magiera-Mularz, K. Guzik, G.  
512 Dubin, T.A. Holak, T. Ossowski, S. Rodziewicz-Motowidło, Ultrasensitive electrochemical  
513 determination of the cancer biomarker protein sPD-L1 based on a BMS-8-modified gold electrode,  
514 *Bioelectrochemistry*, 139 (2021) 107742.
- 515 [46] M. Keough, J.F. McLeod, T. Salomons, P. Hillen, Y. Pei, G. Gibson, K. McEleney, R. Oleschuk, Z.  
516 She, Realizing new designs of multiplexed electrode chips by 3-D printed masks, *RSC Adv.*, 11  
517 (2021) 21600–21606.
- 518 [47] R. Levicky, T.M. Herne, M.J. Tarlov, S.K. Satija, Using Self-Assembly To Control the Structure of  
519 DNA Monolayers on Gold: A Neutron Reflectivity Study, *J. Am. Chem. Soc.*, 120 (1998) 9787–  
520 9792.
- 521 [48] X. Xu, Y. Yu, Q. Hu, S. Chen, L. Nyholm, Z. Zhang, Redox Buffering Effects in Potentiometric  
522 Detection of DNA Using Thiol-Modified Gold Electrodes, *ACS Sens.*, 6 (2021) 2546–2552.
- 523 [49] S.A. Lincy, V. Dharuman, P. Kumar, Ultrasensitive and direct detection of DNA and whole *E coli*  
524 cell at cholesterol gold nanoparticle composite film electrode, *Ionics*, 28 (2022) 1973–1984.
- 525 [50] R.K. Shervedani, A. Farahbakhsh, M. Bagherzadeh, Functionalization of gold cysteamine self-  
526 assembled monolayer with ethylenediaminetetraacetic acid as a novel nanosensor, *Anal. Chim. Acta*,  
527 587 (2007) 254–262.
- 528 [51] G.D. McEwen, F. Chen, A. Zhou, Immobilization, hybridization, and oxidation of synthetic DNA on  
529 gold surface: Electron transfer investigated by electrochemistry and scanning tunneling microscopy,  
530 *Anal. Chim. Acta*, 643 (2009) 26–37.
- 531 [52] R.P. Janek, W.R. Fawcett, A. Ulman, Impedance Spectroscopy of Self-Assembled Monolayers on  
532 Au(111): Sodium Ferrocyanide Charge Transfer at Modified Electrodes, *Langmuir*, 14 (1998) 3011–  
533 3018.
- 534